JACS
JOURNAL OF THE AMERICAN CHEMICAL SOCIETY

Article

pubs.acs.org/JACS

Noise Characteristics of Nanoscaled Redox-Cycling Sensors: Investigations Based on Random Walks

Enno Kätelhön,[†] Kay J. Krause,[†] Pradyumna S. Singh,[‡] Serge G. Lemay,[‡] and Bernhard Wolfrum*[,†,§]

[†]Institute of Bioelectronics (PGI-8/ICS-8) and JARA—Fundamentals of Future Information Technology, Forschungszentrum Jülich, 52425 Jülich, Germany

[‡]MESA+ Institute for Nanotechnology, University of Twente, PO Box 217, 7500 AE Enschede, The Netherlands

[§]Institute of Physics, RWTH Aachen University, 52074 Aachen, Germany

Supporting Information

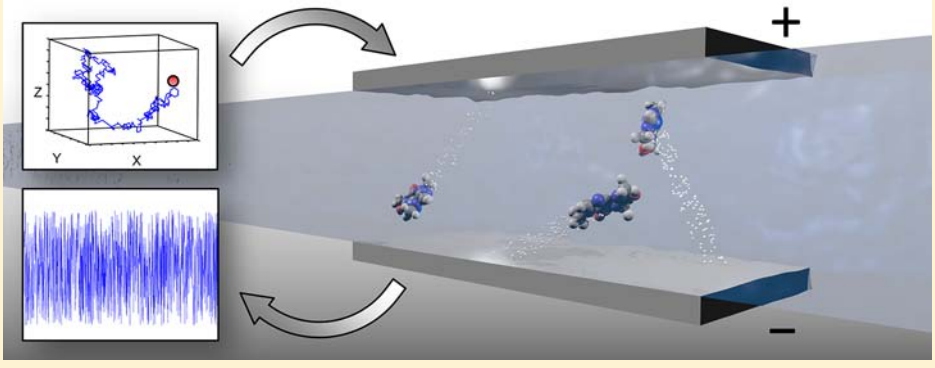

ABSTRACT: We investigate noise effects in nanoscaled electrochemical sensors using a three-dimensional simulation based on random walks. The presented approach allows the prediction of time-dependent signals and noise characteristics for redox cycling devices of arbitrary geometry. We demonstrate that the simulation results closely match experimental data as well as theoretical expectations with regard to measured currents and noise power spectra. We further analyze the impact of the sensor design on characteristics of the noise power spectrum. Specific transitions between independent noise sources in the frequency domain are indicative of the sensor-reservoir coupling and can be used to identify stationary design features or time-dependent blocking mechanisms. We disclose the source code of our simulation. Since our approach is highly flexible with regard to the implemented boundary conditions, it opens up the possibility for integrating a variety of surface-specific molecular reactions in arbitrary electrochemical systems. Thus, it may become a useful tool for the investigation of a wide range of noise effects in nanoelectrochemical sensors.

INTRODUCTION

Following the first description of interdigitated arrays in 1985,[1] the development and characterization of on-chip redox-cycling sensors has evolved to be an active field of research. Since then, a variety of sensor types and designs have been introduced and probed in a wide range of applications.[2−4] Described methods include interdigitated electrodes,[5−9] pore-based approaches,[10−16] and nano- and microcavity devices.[17−23] With respect to measurements involving only a few molecules, nanocavity-based sensors represent one of the current methods of choice. Featuring sensitivity capable of resolving single-molecules[24] as well as a comparably simple fabrication process that is based on standard clean room technology, they have received growing attention during the last years. Typically, sensors consist of two micrometer-scaled electrodes that are separated by tens of nanometers and arranged parallel to each other and the wafer surface. The electrodes can be biased individually and are covered by a passivation layer, while access to the analyte is enabled via small connecting channels. In sensing applications, electrodes are biased to potentials below and above the redox potential of a redox-species under investigation. Molecules can then participate in subsequent oxidation and reduction reactions and, hence, form a measurable current across the electrode gap.

Besides applicability for the detection of redox-active molecules, nanocavity sensors can also be used for spectroscopy applications. In 2009, Zevenbergen et al. introduced a novel spectroscopy approach called electrochemical correlation spectroscopy (ECS).[25] Analogous to fluorescence correlation spectroscopy (FCS), here, the measured current noise is recorded, and its time evolution[25] or amplitude[26] can be analyzed to gain insight into concentration fluctuations as well as adsorption and desorption dynamics of the analyte at the electrodes.[25] Since the electrochemical current of these sensors scales with the number of molecules N that are present in a

Received: December 21, 2012
Published: May 29, 2013

   dx.doi.org/10.1021/ja3121313 | J. Am. Chem. Soc. 2013, 135, 8874−8881

given volume and statistical fluctuations scale with $\sqrt{N}$, noise-to-signal ratios are much improved when few active molecules are located inside the sensor. Due to the nanocavity sensors' ability to operate with ultralow molecule numbers, they represent an ideal platform for noise spectroscopy.

In electrochemical fluctuation spectroscopy, investigations are so far mostly based on noise power spectral densities or autocorrelation descriptions that contain a wide range of information on the respective electrochemical and diffusive processes. However, in many cases, both methods represent a fingerprint of an electrochemical process rather than its full description. Parameters, such as sensor design, adsorption- and desorption rates, inactivation of the analyte, and passivation of the electrodes, may impact the resulting noise characteristics in multiple ways. Therefore, we believe that, with regard to future applications, the technique of ECS can be further advanced by supporting simulations. The simulations may then take into account these diverse effects and determine their influence on the noise spectra, thus leading to a better understanding of the experimental data.

Diffusive processes are often modeled via means of finite element simulation software that is widely available. However, since finite element approaches are based on probability densities for the locations of analyte molecules, only averaged currents can be described, and the modeling of noise remains difficult. For relevance to noise spectroscopy, we base our simulations on stochastic random walks, which simulate every individual molecule's movement. Even though this approach leads to comparably high computational workloads, random walks continuously offer better modeling opportunities due to steady advances in computational power and parallelization. The model further mirrors real-life processes in a detailed, yet simple and demonstrative way. It is easily extendable with regard to effects on the molecular scale, such as adhesion or deactivation of molecules. For these reasons, random walk simulations evolved to a commonly used approach during the last two decades. Successful applications include, the modeling of electron-transfer kinetics,[27] single-molecule electrochemistry,[28] diffusion controlled electrode processes,[29−31] potential-step chronoamperometry,[32] stochastic variations in molecule capturing times at electrodes[33] as well as generator-collector systems based microband electrodes,[34,35] plan-parallel dual disk microelectrodes,[36] and inside concentric spherical electrochemical cells.[32,37]

In a previously published work, we applied a random walk simulation to different geometries and identified two sources of noise: number fluctuation noise that results from the stochastically varying number of molecules in between the two electrodes and redox cycling shot noise, which occurs as a consequence of the diffusive shuttling of molecules in between the electrodes.[38] Based on this, we now provide a significantly more detailed analysis of the noise phenomena in redox-cycling sensors. Using an advanced random walk model based on Monte Carlo simulations in a cubic lattice, we first discuss the accuracy of random walk simulations with regard to the ratio of device size and random walk step width and compare our simulation results to experimental data. Based on these results, we perform a series of simulations for different structure geometries and determine key parameters for spectroscopic applications.

METHODS

The simulation model is based on three fundamental assumptions. First, redox active molecules perform stochastic random walks in accordance with the diffusion equation and are reflected upon collisions with boundaries. Second, each molecule can adopt two different oxidation states, namely the reduced and the oxidized state. Further, molecules change their oxidation state instantly whenever they touch an appropriately biased electrode, i.e., if an oxidized molecule is reflected at a cathode, it changes its state to 'reduced'. A reduced molecule only changes its state at an anode, and oxidized molecules that hit an anode or reduced molecules that hit a cathode do not react. The plane of electron transfer (PET) is approximated to lie at the electrode surface, and kinetic effects are neglected. A detailed analysis of the actual effect of the PET can be found elsewhere.[39−41] Third, redox active molecules do not interact with each other and the electric field of the electrodes. Since nanocavity redox cycling experiments are typically performed at high electrolyte concentrations to ensure a good reference potential throughout the nanofluidic channel, the Debye length is <1 nm for most experimental conditions.

The software is implemented as follows: The simulation is written in C++ and compiled via the GNU Compiler Collection (GCC). Random walks are calculated independently on all available CPUs, while parallel computing is achieved through the application programming interface (API) Open Multi-Processing (OpenMP). During the random walk, each molecule is virtually displaced in time intervals dt by a pseudorandom vector of the length dr. This vector is calculated from three pseudorandom numbers that are obtained via routines taken from the GNU Scientific Library, namely the algorithm mt19937 that is based on the Mersenne Twister code.[42] Hereby, the time dt and the length dr fulfill the following equation that can be derived from the three-dimensional diffusion equation:

$$\mathrm{d}r = \sqrt{6D \cdot \mathrm{d}t} \tag{1}$$

At every step, each Cartesian coordinate of a molecule is either increased or decreased by the fixed distance $\mathrm{d}r' = \mathrm{d}r/\sqrt{3}$. Molecules further move on a static grid, while virtual boundaries are always placed in between two neighboring grid points.

When calculating the random walks, the software processes and records three data traces: the number of reactions at the oxidizing and the reducing electrode (1 and 2) that occur within a predefined sampling interval dT and the average number of redox molecules that are located in between the redox electrodes during the same time (3). Data are then stored in an ASCII file and later processed using the numeric computing environment Matlab.

If not indicated separately, all simulations employ a diffusion constant D of 10^{-9} m^2/s, a virtual sampling rate of 10 kHz, and a spatial step width of 2 nm for the simulated current traces, which exceeds the chosen temporal resolutions of the random walks by orders of magnitude.

RESULTS AND DISCUSSION

Applicability of Random Walk Simulations for Nanoscaled Sensors. In open space, diffusive processes can be easily modeled via stochastic random walks. As long as the step width is kept constant and the spatiotemporal displacement is modeled according to the diffusion equation (see eq 1), the simulation is mathematically identical to the analytical solution, and results can directly be used without further processing. However, the design of simulations becomes more challenging if the space available for diffusion is limited by boundaries. In a random walk simulation, the displacement of each molecule is virtually triggered at a fixed rate 1/dt. Hence, the actual molecule pathway is reduced to a linear movement between a defined start and end position, while all intermediate positions are neglected. Potential collisions at boundaries cannot be considered in such a model. Therefore, any type of boundary condition may impact the simulation results in multiple ways,

dx.doi.org/10.1021/ja3121313 | J. Am. Chem. Soc. 2013, 135, 8874−8881

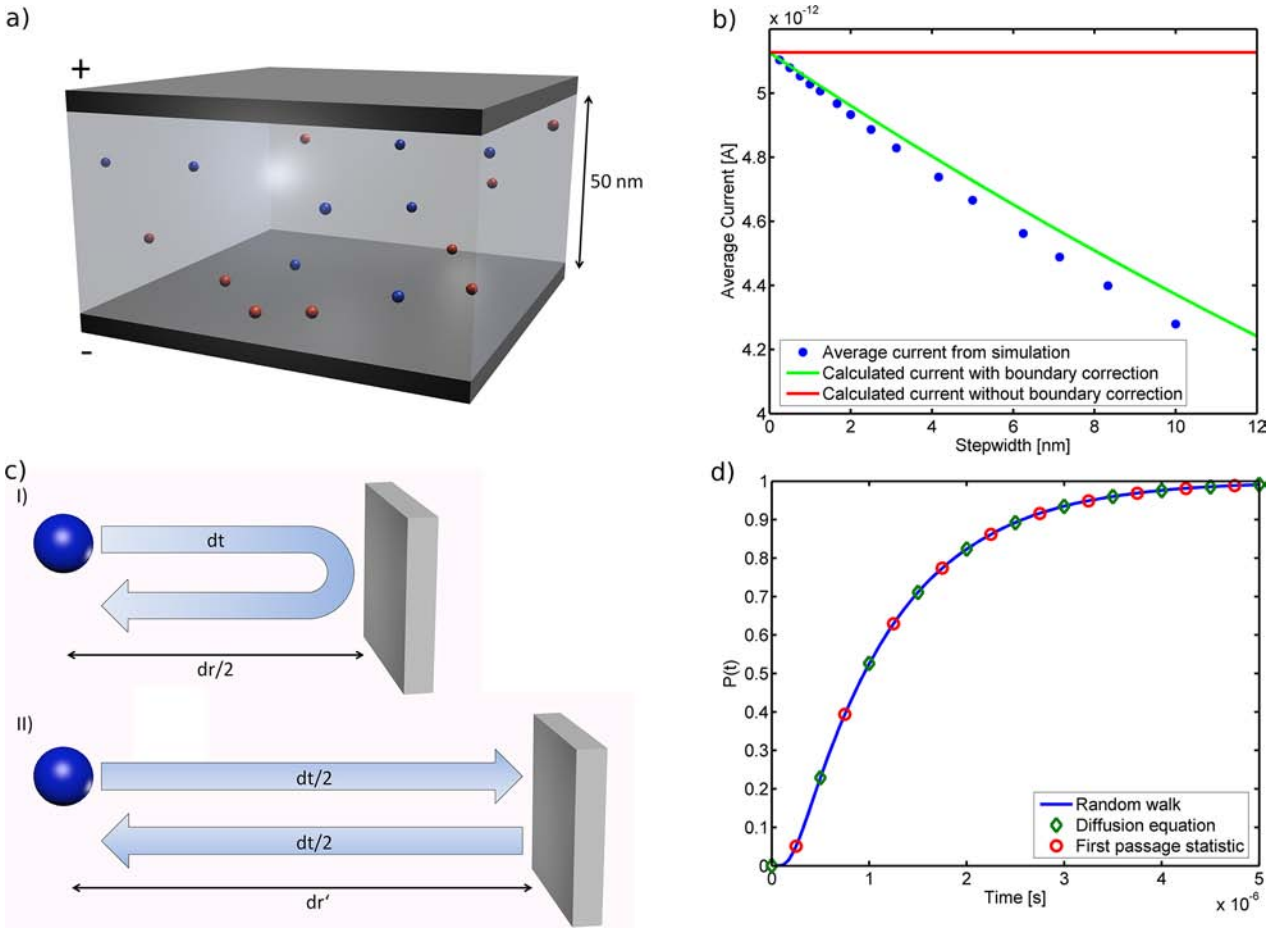

Figure 1. (a) Simple model for the isolated investigation of the redox cycling effect. The sensor consists of two infinite parallel electrodes separated by a nanoscaled gap. (b) Average simulated currents of a sensor consisting of two infinite parallel electrodes at a distance of 50 nm. The red graph represents the theoretical result, the blue graph shows the simulated average current at one electrode, and the green graph shows the corrected current according to eq 7. The random walk simulation used 80 molecules, and the charge transfer per reaction amounts to the elementary charge. (c) Two reflection models: (I) Pathway of a single step dr at a simple reflecting boundary within the time interval dt. (II) Corrected boundary position according to diffusion equation. The random walk is subdivided into two steps of the spatial step width dr' and the temporal step width dt/2. (d) Cumulated reaction probability of a molecule that is located in between two parallel absorbing boundaries that are separated by a distance of 100 nm. The molecule is released centrally at the time $t = 0$. The probability was calculated in three different ways.

depending on the simulated geometry and the reflection algorithm chosen.

In order to quantify the impact of this effect on our simulations, we choose a simple geometry for a parameter screening: A model of two infinite parallel plates that represents electrodes biased for redox cycling (see Figure 1a). A set of 80 active molecules at random oxidation states is released uniformly distributed between the electrodes. The electrode response is then recorded for a time interval of 0.1 s. The simulation is repeated several times with varied step widths, and the average current is individually determined for each repetition. Simulation results can then be compared to an analytical solution for the average current that can be derived from the one-dimensional diffusion equation: On average, the transmission of one molecule's redox charge load from one electrode to the other requires twice the time, T_{trans}, it takes for a molecule to diffusively travel the distance h between the electrodes. Analogous to eq 1, in the one-dimensional case this time can be calculated as follows:

$$T_{trans} = \frac{h^2}{2D} \tag{2}$$

Hence, the average current per redox-active molecule in between the electrodes is given by:

$$I_{Molecule} = \frac{D \cdot q_{molecule}}{h^2} \tag{3}$$

where $q_{molecule}$ represents the charge that can be exchanged by one molecule.[18,43]

The result of this model can be seen in Figure 1b, which compares the theoretically calculated current with the values obtained from simulations that use various step widths. In the plot one can find an increasing underestimation of the simulated current at higher step widths, which relates to the discrete nature of the random walk approach that disregards intermediate positions of a molecule's trajectory in between two subsequent positions in the simulation. One effect is particularly relevant for the simulation of nanoelectrochemical effects: Whenever a molecule is located in immediate proximity to a reflecting boundary and follows a reflected pathway (as seen in see Figure 1c, (I)), the molecule's distance to the boundary is underestimated. During this time interval dt, the molecule first approaches the electrodes while passing the distance dr/2. Then it is reflected and again passes the distance

dx.doi.org/10.1021/ja3121313 | J. Am. Chem. Soc. 2013, 135, 8874−8881

$dr/2$ back toward its initial position. However, since the molecule's diffusive pathway is not linear in time, the reflection has to be treated as two individual steps that are performed within the interval dt and that feature a different spatial step width dr', see Figure 1c, (II). Based on the one-dimensional diffusion equation:

$$dr_{1D} = \sqrt{2D \cdot dt} \tag{4}$$

we can calculate the length of dr' as follows:

$$dt = \frac{dr_{1D}^{\ 2}}{2D} = \frac{2dr'_{1D}{}^{2}}{2D} \tag{5}$$

This leads to an expression for dr':

$$dr' = \frac{dr_{1D}}{\sqrt{2}} \tag{6}$$

We can now calculate an effective distance h' between the two electrodes that is corrected for the discrepancy in the step size at both boundaries:

$$h' = h - 2\frac{dr_{1D}}{2} + 2dr'_{1D} = h + (\sqrt{2} - 1)dr_{1D} \tag{7}$$

Based on this formula and eq 3, we can calculate the deviation in the simulated current that is caused by this effect. The so-predicted current explains most deviations caused by the discrete nature of the random walk, as illustrated in Figure 1b. In the following, however, we correct all simulated currents according to the deviation that we measured between the simulated data and the theoretical value that was found via eq 3.

In conclusion, by running the simulation that is sketched in Figure 1a, we could show that the average value of T_{trans} in our simulation closely matches the theoretical value at small step widths and that we can correct our simulation results in case of longer step widths. However, its statistical distribution has not been validated, yet. Therefore, we run a second, slightly modified simulation in order to confirm the statistical distribution of T_{trans}: We release 170 000 molecules centered in between the electrodes, while we record the time interval until they hit one of the electrodes for the first time. Out of this data, we calculate the accumulated reaction probability as a function of the time since the molecules' release. We compare our results to two analytical solutions: first, the solution of the one-dimensional diffusion equation (see Supporting Information) and second a discrete analytical approach based on the Gambler's Ruin problem that was previously introduced by Zevenbergen et al. to describe the first passage of molecules in a one-dimensional nanofluidic channel.[17] In our context, the model describes the absorption probability $P(n)$ of a random walker that is released centrally in between two absorbing boundaries. Hereby, n describes the number of steps that the molecule performed since its release and a is the distance between the two boundaries in steps:

$$P(n, a) = \frac{2}{a}\sum_{v=1}^{a-1} \cos^{n-1}\frac{\pi v}{a} \sin\frac{\pi v}{a} \sin\frac{\pi v}{2} \tag{8}$$

As can be seen in Figure 1d, all three models are in close agreement. Hence, our simulation offers good applicability for the modeling of statistical processes.

Comparison Simulation and Experiment. In order to validate our model, we compare our simulations with experimentally obtained data. Here, we use a nanofluidic device that was described by Zevenbergen et al. in 2009.[19] In short, this device features a nanochannel (26 μm × 1.5 μm × 50 nm) and two Pt electrodes that are located centrally on top and below the nanochannel and overlap in an area of 10 × 1.5 μm. The sensor further has two access channels (1 μm × 1 μm × 550 nm) at either end that provide diffusive access from the bulk reservoir to the nanochannel. Measurements were performed in a 50 μM $Fc(MeOH)_2$ solution after functionalizing the electrodes with 3-mercaptopropionic acid (3-MPA). Exact parameters of this experiment have been described elsewhere;[26] detailed information on the data processing can be found in Supporting Information. The design used in the simulation can be found in Figure 2a. It is based on the symmetry of the real-life sensor design; however, a simplification is introduced: We use the system's symmetry and implement only one-half of the sensor. Since molecules do

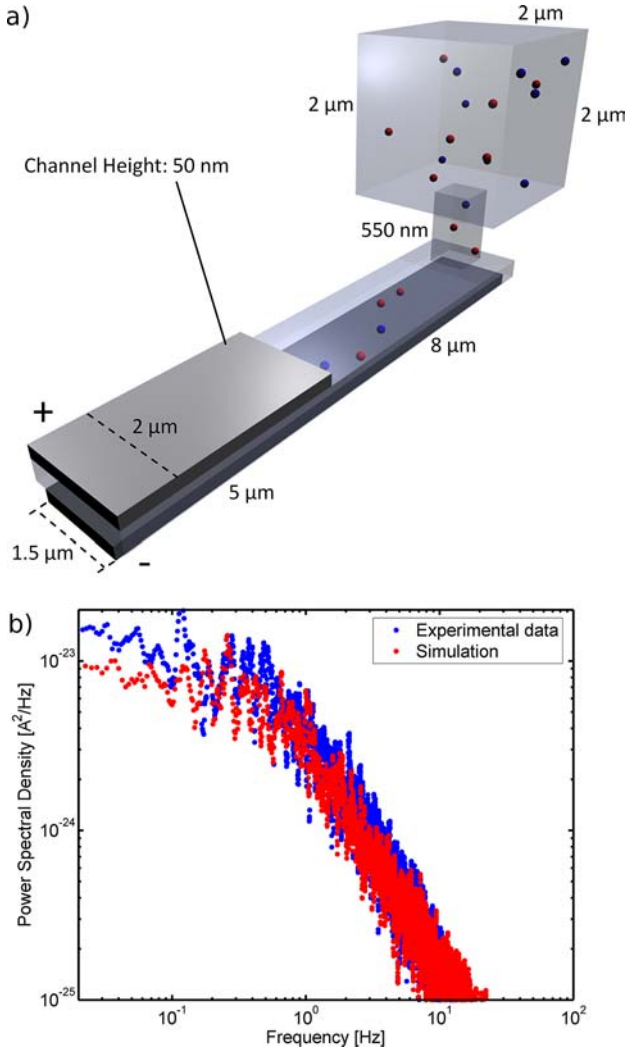

Figure 2. (a) Sketch of the model that is used for simulation in order to compare simulated to experimental data. The sensor consists of two parallel electrodes separated by a nanocavity. Access to a small bulk reservoir is enabled via an access channel at the end of the nanocavity. (b) Power spectral densities obtained from simulation (red) and experiment (blue). Our simulation uses 200 individual random walks and a diffusion constant of 0.67×10^{-9} m^2/s. The temporal step width is 10^{-7} s, and the sampling interval is 2 ms. Data were filtered using a moving average filter.

dx.doi.org/10.1021/ja3121313 | J. Am. Chem. Soc. 2013, 135, 8874−8881

not interact with each other and reflect at the intersecting plane, this system is identical to the experiment as long as the concentration is doubled.

As we will show later, the amplitude of the power spectral density at low frequencies scales linearly with the number of molecules inside the sensor. Since the number of molecules involved in the experiment exceeds the number of molecules that can be simulated in reasonable time on our system employed, we utilize this linear relationship in order to derive data that match the experimental parameters from a simulation that uses fewer molecules. When doing so, we first calculate the number of molecules that contribute to the experimentally obtained current by dividing the average measured current by the theoretical current contribution of a single molecule (see eq 3). By this means, we estimate the average number of molecules inside the sensor to ∼19.760 and scale the amplitude of the simulated power spectral density accordingly. Furthermore, we correct the deviation caused by adsorption effects. These effects generally lead to a rescaling of the frequency axis by a constant factor in the power spectral density, while the magnitude of the shift is known from literature.[25,26] In short, adsorption inside the nanochannel slows down the average speed of the active molecules' diffusive movement along the channel, leading to an effective diffusion constant that is smaller than the diffusion constant in bulk solution. For the current design, the frequency axis is scaled by a factor of 0.5 according to the calculations by Singh et al.[26]

Figure 2b shows the so obtained simulated data together with recordings from the experiment. As it can be seen in the figure, our simulation closely reproduces the experiment. However, a small underestimation of the experimentally obtained spectra can be found in the low-frequency regime of 0.01−0.1 Hz. We attribute this derivation to a slow drift in the current caused by our measurement setup during the experiment.

Investigations of Noise Spectra. As mentioned previously, nanocavity sensors exhibit two intrinsic types of noise that result from different sources: the molecules shuttling between the electrodes and the molecules entering and leaving the sensor's detection region. In the following, we first treat both effects separately and investigate various parameter dependencies. Later the full spectrum of a typical nanocavity sensor is modeled.

Redox-Cycling Shot Noise. Shot-like redox-cycling noise results from the thermal motion of redox-active molecules inside the sensor. Since molecules shuttle diffusively in between the electrodes, the measured overall current across the gap always depends on the individual trajectories of all molecules. As each trajectory is stochastic, the measured current is also subject to stochastic fluctuations. In order to quantize their impact on the spectra, we simulate the power spectral density of a varied number of molecules in the above-mentioned parallel-plates geometry (see Figure 1a). Since the number of molecules inside the sensor is held constant in this model, the obtained noise is exclusively caused by redox cycling shot noise; noise from concentration fluctuations cannot occur. The corresponding power spectral densities can be seen in Figure 3.

The figure demonstrates that, as expected for the relatively low frequencies investigated here,[38] the redox-cycling shot noise exhibits a white noise characteristic, i.e., the noise power at a certain frequency is independent of the frequency itself. This white noise characteristic is also independent from the number of molecules inside the sensor; however, the amplitude of the noise power varies with the concentration. As it can be seen in the inset, the average values of the power spectral densities scale linearly with the number of molecules inside the sensor. This result is in line with theoretical considerations: In molecular processes that are dominated by Poisson statistics, fluctuations generally scale with the square root of the number molecules involved. Hence, their power scales linearly with the number of molecules.

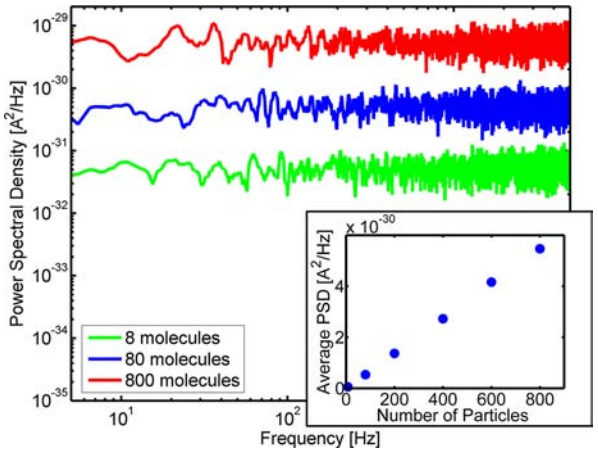

Figure 3. Top: Simulated power spectral densities of the currents in the parallel plates model. The pictured simulations use 8, 80, and 800 molecules (green, blue, red), and the data are filtered using a moving average filter. Bottom: Average values of each power spectral density as a function of the number of molecules inside the sensor.

In the context of the spectroscopy methods described below, redox cycling shot noise contributes one characteristic number: The average power spectral density S_1 of the white noise spectra, which both depends on the number of molecules N inside the sensor and scales with h^{-2}, as previously shown in eq 3. Due to its dependency on N, the contribution of this type of noise is small at low concentrations and, hence, difficult to observe in measurements like in single-molecule detection.[28] However, the magnitude of redox-cycling shot noise increases at higher concentrations and larger electrode surfaces as can be seen in Figure 3.

Number Fluctuation Noise. In addition to redox cycling shot noise, nanocavity redox-cycling devices exhibit another type of noise that results from fluctuations in the number of molecules inside the sensor.[25,26] Due to the sensors strong amplification of the individual faradaic currents caused by each single molecule, small statistical fluctuations in the number of analyte molecules cause a significant part of the overall noise on the current.

For quantization of the noise character that results from this effect, we implement a design similar to our real-life redox-cycling sensors in our simulation model.[20] The simulated design features two circular electrodes that are 15 μm wide and located in parallel to each other. They are separated by a 50 nm wide cavity of the same lateral size. The setup is integrated into an 850 nm thick passivation layer that is interpenetrated by a circular access channel, centrally with regard to the electrodes positions. Furthermore, a cylindrical bulk reservoir is added to the system centrally at the opening of the access channel, see Figure 4a.

Since the overall electrode current is always affected by both noise sources—the redox cycling shot noise and the diffusion number fluctuation noise—we additionally record the average number of molecules that are located in between the electrodes

dx.doi.org/10.1021/ja3121313 | J. Am. Chem. Soc. 2013, 135, 8874−8881

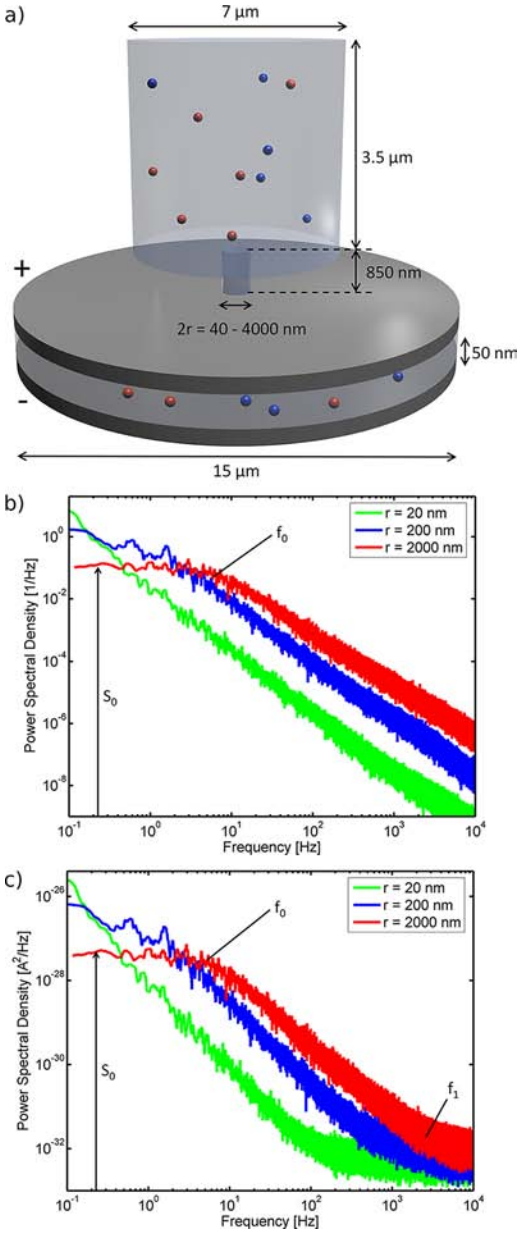

Figure 4. (a) Sketch of the model that is used to investigate the number fluctuation noise. The sensor consists of two parallel electrodes separated by a nanocavity. Access to a small bulk reservoir is enabled via an access channel that interpenetrates the top electrode. (b) Power spectral density of the number of molecules between the electrodes at different sensor openings. This corresponds to the spectral density of the number fluctuation noise alone. The simulation was calculated for radii of 20 nm (green), 200 nm (blue), and 2000 nm (red). The traces magnitude was normalized to an average of one molecule inside the sensor. The model uses 80 molecules, and data were filtered using a moving average filter. (c) Power spectral density of the simulated current for different radii of the sensor opening. This includes both shot noise and number fluctuation noise. The crossover from between which of these sources of noise is dominant is indated by the label f_1. Parameters match the ones chosen in Figure 4b.

within each sampling interval. By analyzing this additional trace, we can investigate the impact of fluctuations in the number of molecules inside the sensor separately from the redox cycling shot noise. Assuming the system under investigation remains in a state of equilibrium, the character of these fluctuations depends on only two factors: the nature of the analyte molecules' diffusive movement and the geometry of the sensor. In particular, the geometry of the space that is enclosed by the electrodes and its connection to the bulk reservoir play an important role. In our simulations, we probe the impact of this design feature by varying the diameter of the sensor access channel to the bulk reservoir. By this means, the overall surface area of this diffusive link to the nanocavity is varied. Plots showing the power spectral densities of the number of molecules that were obtained at varied surface areas of the diffusive interconnection between the space enclosed by the electrodes and the other parts of the sensor can be found in Figure 4b.

In the plot, we can find a characteristic feature that was formerly described by Zevenbergen et al. and Singh et al.[25,26] The graphs show a flat plateau in the low-frequency regime, which spreads up to a transition frequency f_0. Above this frequency the power spectral density drops according to a power law, which can be seen by the linear trace in the logarithmic plot. Furthermore, one can find that the level of the noise S_0 at the plateau decreases with the diameter of the sensor opening, while f_0 moves to lower frequencies. Besides this offset in frequency and level, the shape of the power spectral density remains unchanged by the variation of the coupling between the sensor and the reservoir, and neither is the character of the power law drop above the transition frequency f_0 affected.

For spectroscopy applications, one can make use of the fact that both f_0 and S_0 are dependent on this design feature. Hence one can employ the average value S_0 of the low-frequency plateau as well as the frequency f_0 for the specification of the diffusive connection between the interelectrode area and the bulk reservoir in this idealized model.

Current Noise in Nanocavity Sensors. The sensor's current is subject to both sources of noise, the redox cycling shot noise, and the number fluctuation noise. This can be seen in the plot of the power spectral densities from the current traces (see Figure 4c).

The plot illustrates that the low-frequency domain is fully dominated by the number fluctuation noise. As it can be expected from Figure 3, the redox cycling shot noise in this regime is too small to significantly contribute to the current noise. However, since the fluctuation concentration noise drops with a power law at higher frequencies, there is another, second transition frequency f_1 that occurs at the frequency, at which the magnitude of the fluctuation concentration noise drops below the level of the white noise spectra of the redox cycling shot noise. Hence, the noise spectra of the current can be considered to be a sum of the two other noise sources: redox cycling shot noise and number fluctuation noise. The two characteristic values S_0 and S_1 can be found in the graph and be used as reference values for spectroscopic applications. Furthermore, the value f_1 of the second transition frequency can be obtained from the simulation. This value can be used to determine the ratio of the impacts of the two noise sources. Since the magnitudes of both noise sources scale equally with the number of molecules n in the system and thus the analyte concentration, f_1 provides a direct measure for the sensor's diffusive access to the bulk reservoir, which is independent from the concentration and only requires the knowledge of the inter electrode distance h.

Potential applications can be found particularly for gated redox currents[44] with nanoporous devices. Since f_1 strongly depends on the size of the connecting channel and increases

dx.doi.org/10.1021/ja3121313 | J. Am. Chem. Soc. 2013, 135, 8874−8881

with its diameter, devices that feature only small connecting channels between the active area of the sensor and the bulk reservoir are best suited to avoid exceeding the measurable frequency range. Furthermore, when this requirement is met, changes in the diffusive coupling between the sensor and the bulk reservoir are reflected in the sensor noise. Hence, sensing approaches that can measure blocking of the sensor's access channels, for example, via an antibody−antigen interaction or a chemical modification of the channel's surface, can be based on this spectroscopy method.

CONCLUSIONS

We have presented a simulation framework of the noise characteristics of nanocavity redox cycling sensors. We first discussed the applicability of these simulations by comparison to theoretical results and quantified the impact of the step width used in the simulation on the result. Then, we compared our simulation to experimental data and demonstrated the applicability to modeling real-life sensors. In the last part of this work, we focused on the two characteristic sources of noise: redox cycling shot noise and number fluctuation noise. We described the dependency of redox cycling shot noise on the system's parameters in detail. Then we reproduced the main characteristics of noise caused by concentration fluctuations in a nanofluidic sensor. Furthermore, we analyzed the impact of variations in the connection of the sensor to the bulk reservoir on the noise spectrum and found that the number fluctuation noise level in the low-frequency regime scales inversely with the diffusive access to the bulk reservoir. Both sources of noise are present in electrochemical current noise, where the number fluctuation noise dominates the low-frequency regime and redox cycling shot noise dominates the higher frequencies. Since only the number fluctuation noise is affected by the strength of the diffusive coupling to an external reservoir, one can utilize the transition frequency to determine this coupling parameter.

Based on simple model assumptions, random walk simulations offer a fast and easy option to obtain noise power spectral densities of complex sensor designs that are difficult to attain otherwise. Due to the model's simple structure, it can be easily extended toward other effects like adsorption or electrode passivation and, hence, offer an insight into more complex spectroscopy methods for future applications. Thus, we disclose our source code to the scientific community as a tool for analyzing data from nanoelectrochemical sensors exhibiting advanced boundary conditions.

ASSOCIATED CONTENT

Supporting Information

This material is available free of charge via the Internet at http://pubs.acs.org.

AUTHOR INFORMATION

Corresponding Author

b.wolfrum@fz-juelich.de

Notes

The authors declare no competing financial interest.

ACKNOWLEDGMENTS

We gratefully acknowledge funding by the Helmholtz Young Investigators Program, NWO, and ERC. We thank Martin Hüske and Michael Pabst for helpful discussions.

REFERENCES

(1) Sanderson, D. G.; Anderson, L. B. *Anal. Chem.* **1985**, *57*, 2388−2393.
(2) Rassaei, L.; Singh, P. S.; Lemay, S. G. *Anal. Chem.* **2011**, *83*, 3974−3980.
(3) Kätelhön, E.; Wolfrum, B. *Rev. Anal. Chem.* **2012**, *31*, 7−14.
(4) Batchelor-McAuley, C.; Dickinson, E. J. F.; Rees, N. V.; Toghill, K. E.; Compton, R. G. *Anal. Chem.* **2011**, *84*, 669−684.
(5) Chidsey, C. E.; Feldman, B. J.; Lundgren, C.; Murray, R. W. *Anal. Chem.* **1986**, *58*, 601−607.
(6) Feldman, B. J.; Murray, R. W. *Anal. Chem.* **1986**, *58*, 2844−2847.
(7) Aoki, K.; Morita, M.; Niwa, O.; Tabei, H. *J. Electroanal. Chem.* **1988**, *256*, 269−282.
(8) Ino, K.; Nishijo, T.; Arai, T.; Kanno, Y.; Takahashi, Y.; Shiku, H.; Matsue, T. *Angew. Chem., Int. Ed.* **2012**, *51*, 6648−6652.
(9) Ino, K.; Kanno, Y.; Nishijo, T.; Goto, T.; Arai, T.; Takahashi, Y.; Shiku, H.; Matsue, T. *Chem. Commun.* **2012**, *48*, 8505−8507.
(10) Henry, C. S.; Fritsch, I. *J. Electrochem. Soc.* **1999**, *146*, 3367−3373.
(11) Henry, C. S.; Fritsch, I. *Anal. Chem.* **1999**, *71*, 550−556.
(12) Vandaveer, W. R., IV; Woodward, D. J.; Fritsch, I. *Electrochim. Acta* **2003**, *48*, 3341−3348.
(13) Neugebauer, S.; Müller, U.; Lohmüller, T.; Spatz, J. P.; Stelzle, M.; Schuhmann, W. *Electroanalysis* **2006**, *18*, 1929−1936.
(14) Neugebauer, S.; Stoica, L.; Guschin, D.; Schuhmann, W. *Microchim. Acta* **2008**, *163*, 33−40.
(15) Lohmüller, T.; Müller, U.; Breisch, S.; Nisch, W.; Rudorf, R.; Schuhmann, W.; Neugebauer, S.; Kaczor, M.; Linke, S.; Lechner, S.; Spatz, J.; Stelzle, M. *J. Micromech. Microeng.* **2008**, *18*, 115011.
(16) Hüske, M.; Wolfrum, B. *Phys. Status Solidi A* **2011**, *208*, 1265−1269.
(17) Zevenbergen, M. A. G.; Krapf, D.; Zuiddam, M. R.; Lemay, S. G. *Nano Lett.* **2007**, *7*, 384−388.
(18) Wolfrum, B.; Zevenbergen, M.; Lemay, S. *Anal. Chem.* **2008**, *80*, 972−977.
(19) Zevenbergen, M. A. G.; Wolfrum, B. L.; Goluch, E. D.; Singh, P. S.; Lemay, S. G. *J. Am. Chem. Soc.* **2009**, *131*, 11471−11477.
(20) Kätelhön, E.; Hofmann, B.; Lemay, S. G.; Zevenbergen, M. A. G.; Offenhäusser, A.; Wolfrum, B. *Anal. Chem.* **2010**, *82*, 8502−8509.
(21) Zhu, X.; Ino, K.; Lin, Z.; Shiku, H.; Chen, G.; Matsue, T. *Sens. Actuators, B* **2011**, *160*, 923−928.
(22) Straver, M. G.; Odijk, M.; Olthuis, W.; van den Berg, A. *Lab Chip* **2012**, *12*, 1548−1553.
(23) Lewis, P. M.; Sheridan, L. B.; Gawley, R. E.; Fritsch, I. *Anal. Chem.* **2010**, *82*, 1659−1668.
(24) Zevenbergen, M. A. G.; Singh, P. S.; Goluch, E. D.; Wolfrum, B. L.; Lemay, S. G. *Nano Lett.* **2011**, *11*, 2881−2886.
(25) Zevenbergen, M. A. G.; Singh, P. S.; Goluch, E. D.; Wolfrum, B. L.; Lemay, S. G. *Anal. Chem.* **2009**, *81*, 8203−8212.
(26) Singh, P. S.; Chan, H.-S. M.; Kang, S.; Lemay, S. G. *J. Am. Chem. Soc.* **2011**, *133*, 18289−18295.
(27) White, R. J.; White, H. S. *Anal. Chem.* **2005**, *77*, 214−220.
(28) Singh, P. S.; Kätelhön, E.; Mathwig, K.; Wolfrum, B.; Lemay, S. G. *ACS Nano* **2012**, *6*, 9662−9671.
(29) Nagy, G.; Sugimoto, Y.; Denuault, G. *J. Electroanal. Chem.* **1997**, *433*, 167−173.
(30) Nagy, G.; Denuault, G. *J. Electroanal. Chem.* **1997**, *433*, 175−180.
(31) Liang, S.; Guo, Q.; Dong, X. *J. Electroanal. Chem.* **2009**, *633*, 235−239.
(32) Cutress, I. J.; Dickinson, E. J. F.; Compton, R. G. *J. Electroanal. Chem.* **2011**, *655*, 1−8.
(33) Liang, S.; Dong, X. *Electroanalysis* **2011**, *23*, 1447−1453.
(34) Licht, S.; Cammarata, V.; Wrighton, M. S. *Science* **1989**, *243*, 1176−1178.
(35) Licht, S.; Cammarata, V.; Wrighton, M. S. *J. Phys. Chem.* **1990**, *94*, 6133−6140.
(36) Baur, J. E.; Motsegood, P. N. *J. Electroanal. Chem.* **2004**, *572*, 29−40.

(37) White, R. J.; White, H. S. *Langmuir* **2008**, *24*, 2850−2855.
(38) Kätelhön, E.; Wolfrum, B. *Phys. Status Solidi A* **2012**, *209*, 881−884.
(39) Smith, C. P.; White, H. S. *Anal. Chem.* **1992**, *64*, 2398.
(40) He, R.; Chen, S.; Yang, F.; Wu, B. *J. Phys. Chem.* **2006**, *110*, 3262−3270.
(41) Dickinson, E. J. F.; Compton, R. G. *J. Electroanal. Chem.* **2011**, *661*, 198−212.
(42) Matsumoto, M.; Nishimura, T. *ACM Trans. Model. Comput. Simul.* **1998**, *8*, 3−30.
(43) Fan, F.-R. F.; Bard, A. J. *Science* **1995**, *267*, 871−874.
(44) Liu, G.; Sun, C.; Li, D.; Song, S.; Mao, B.; Fan, C.; Tian, Z. *Adv. Mater.* **2010**, *22*, 2148−2150.